Dalton Transactions

ROYAL SOCIETY OF CHEMISTRY

COMMUNICATION

View Article Online
View Journal | View Issue

Cite this: *Dalton Trans.*, 2026, **55**, 72

Received 5th November 2025,
Accepted 4th December 2025

DOI: 10.1039/d5dt02653a

rsc.li/dalton

Integration of a metallic interstitial co-catalyst (Ni_3Mo_3N) onto CdS nanorods accelerated charge separation and efficient photocatalytic hydrogen evolution

Lu Chen, Kaijie Zhang, Yule Sun, Ruowen Liang, Guiyang Yan * and Renkun Huang*

A metallic interstitial compound Ni_3Mo_3N was synthesized as a co-catalyst modified CdS nanorod for the first time. Photocatalytic studies show that the efficient charge separation and transfer from CdS to Ni_3Mo_3N enables high visible-light-driven hydrogen evolution at 6.56 mmol g^{-1} h^{-1}. The Schottky heterojunction between CdS and Ni_3Mo_3N might be the key factor for the high photocatalytic activity.

1. Introduction

Photocatalytic water splitting into hydrogen is a promising route for transforming solar energy into clean and sustainable chemical fuel.[1–3] A typical water-splitting photocatalyst contains two components: a light-harvesting semiconductor and a hydrogen evolution co-catalyst.[4,5] The semiconductor absorbs photons and converts them to electron–hole pairs (*i.e.*, carriers), while the co-catalyst plays a crucial role in the photocatalytic process: accelerating the charge separation of photoexcited charge carriers at the co-catalyst/semiconductor interface, providing active sites to suppress back reaction, and lowering the activation energy of the hydrogen evolution reaction.

Recently, cadmium sulfide (CdS) has been proven to be one of the most promising candidate semiconductors for visible-light response photocatalytic properties, owing to its narrow band gap (E_g = 2.4 eV) and appropriate conduction band edge.[6–8] However, the bare CdS exhibited low photocatalytic efficiency due to its photocorrosion and fast recombination of photogenerated electron–hole pairs.[9] To overcome these bottlenecks, a co-catalyst loaded onto semiconductor surfaces not only serves as an active site for hydrogen evolution but also contributes to promoting the charge transfer. So far, platinum (Pt) has been proven to be the most efficient noble metal co-catalyst, benefiting from its small overpotentials and low Fermi energy levels. However, its widespread application is limited by their high cost and rare earth-abundance. Therefore, it is a central and urgent issue to find novel highly efficient and noble-metal-free co-catalyst. To date, transition-metal nonoxides (*e.g.*, carbides, sulfides, phosphides and nitrides) have been extensively studied as efficient co-catalysts due to their d-band states' resemblance to platinum.[10–14] Among them, transition-metal nitride is highlighted in view of its superior activity and high stability, which makes it a very promising candidate for photocatalytic hydrogen evolution.[15,16] Typically, Ni–Mo bimetallic nitrides, a class of metallic interstitial compounds, have attracted much attention in the field of electrocatalysis.[17] For example, Ren and co-workers reported the use of Ni–Mo nitrides (NiMoN) nanorods as electrocatalysts for hydrogen evolution, with reaction activity close to that of Pt/C electrodes.[18] The outstanding performance was ascribed to their excellent electronic conductivity and low adsorption free energy of H*, which facilitates electron transportation to the absorbed protons and reduction to hydrogen release. However, to the best of our knowledge, Ni–Mo bimetallic nitride (Ni_3Mo_3N) have not been employed as the co-catalyst for photocatalytic hydrogen evolution.

In this work, we report for the first time noble-metal-free Ni_3Mo_3N as a highly co-catalyst for photocatalytic H_2 production under visible light. After Ni_3Mo_3N (10%) was coupled with CdS, the H_2 evolution activity is remarkably increased to 6.56 mmol g^{-1} h^{-1}, which was about 25 times higher than that of bare CdS sample. Moreover, the Ni_3Mo_3N/CdS composite showed excellent stability during the photocatalytic hydrogen evolution reaction for six consecutive cycles. A series of photoelectrochemical characterizations and Kelvin probe measurements prove that the Ni_3Mo_3N nanoparticles anchoring on the CdS surface facilitates photoinduced electron–hole pair separation and transfer, and therefore contributing to the improved photocatalytic activity for hydrogen evolution rate.

Fig. S1a shows the XRD pattern of the obtained orthorhombic Ni_3Mo_3N nanoparticles and no other impurities such as Ni and Ni_3N are detected in the sample. As shown in Fig. S1b, all diffraction peaks of CdS can be corresponded to

Department of Chemistry, Fujian Province University Key Laboratory of Green Energy and Environment Catalysis, Ningde Normal University, Ningde 352100, PR China

hexagonal CdS. Compared with pristine CdS, the diffraction peak at 40.7° can be clearly seen in the Ni_3Mo_3N/CdS composites, which corresponds to the (221) plane of Ni_3Mo_3N, indicating that Ni_3Mo_3N was successfully anchored onto CdS. The TEM images clearly show that the Ni_3Mo_3N nanoparticle and CdS are in close contact with each other (Fig. 1a). The HRTEM image further observed show lattice spacings at 0.32 and 0.30 nm, which corresponds to the (101) and (021) diffraction planes of CdS and Ni_3Mo_3N (Fig. 1b). In addition, the corresponding EDX mapping of the Ni_3Mo_3N/CdS composite as shown in Fig. 1c clearly indicates the existence of Cd, S, Ni, Mo and N elements in the sample and the uniform distribution of Ni, Mo and N elements. Collectively, it is conclusive from these experimental results that the Ni_3Mo_3N nanoparticle was successfully loaded onto the CdS nanorod, forming heterojunction structure, and thus improves the rate of water reduction reaction.

X-ray photoelectron spectroscopy (XPS) reveals the presence of Cd, S, Ni and Mo elements in Ni_3Mo_3N/CdS composite. This is in accordance with the TEM data. The high-resolution XPS spectra of Cd 3d and S 2p show that, the binding energy of Cd 3d and S 2p shift slightly toward higher binding energy, which are attributed to the increase in electronic density in CdS after loading Ni_3Mo_3N and a strong interaction between CdS and Ni_3Mo_3N.[14,19] For the high-resolution XPS of Ni 2p, the peak at 853.9 eV was assigned to the Ni^+ species in Ni–N,[5,20] while the peaks located at 856.7 and 871.6 eV are ascribed to Ni $2p_{3/2}$ and Ni $2p_{1/2}$ of Ni^{2+} species.[21] Furthermore, the two additional peaks at 862.6 and 876.2 eV are the relevant satellite peaks, demonstrating the existence of surface partial oxidation of the Ni_3Mo_3N/CdS sample. In Fig. S2d, the binding energies of Mo 3d was observed at 228.1 eV could be attributed to the metal-nitride.[22] The peak located at 225.9 eV corresponding to the characteristic binding energy of S 2s in sulfides.[23,24] The peaks located at 227.2, 231.3, 232.3 and 235.4 eV are assigned to Mo^{4+} and Mo^{6+} due to the surface oxidation of Ni_3Mo_3N.[25–28] In addition, the N 1s peak intensity is very low for Ni_3Mo_3N (10 wt%)/CdS, and this may be due to the small amount of Ni_3Mo_3N in the composite.[29–31]

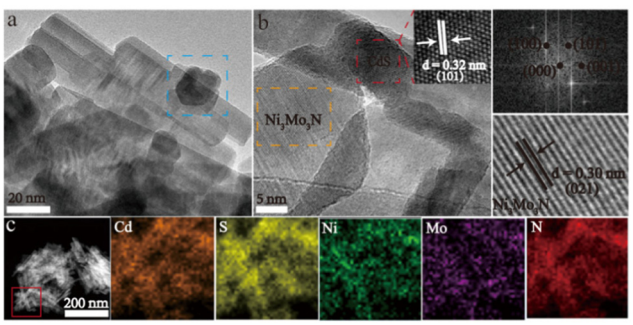

Fig. 1 (a and b) TEM and HRTEM images of the Ni_3Mo_3N (10 wt%)/CdS sample and (c) EDX elemental mapping images of the Ni_3Mo_3N (10 wt%)/CdS sample.

The UV-vis absorption spectra of the photocatalysts were employed to measure their light-harvesting abilities. As shown in Fig. 2a, there is a gradually enhanced absorption in the whole visible light region with the increase in the content of Ni_3Mo_3N. This can be attributed to the black metallic Ni_3Mo_3N that absorbs all visible photons. Meanwhile, the behavior of charge trapping and separation in the CdS and Ni_3Mo_3N/CdS composites was evaluated using photoluminescence. It can be observed that the Ni_3Mo_3N co-catalyst loading results in a higher degree of quenching of CdS nanorod PL intensity, indicating that the recombination efficiency of the photogenerated electron–hole pairs in the CdS nanorods is greatly suppressed. This is reasonable because Ni_3Mo_3N is able to accept and shuttle the photogenerated electrons from CdS because of its excellent electron conductivity and strong interaction between Ni_3Mo_3N and CdS. Moreover, the Ni_3Mo_3N/CdS composite shows a higher photocurrent density than bare CdS. In addition, Ni_3Mo_3N/CdS exhibited a smaller semicircle than CdS in the Nyquist plots from electrochemical impedance spectroscopy (EIS), revealing that photoexcited charge carrier separation was promoted after the Ni_3Mo_3N loading.

To measure the photocatalytic activity of the Ni_3Mo_3N/CdS composites, we carried out the photocatalytic hydrogen evolution experiments using Na_2S and Na_2SO_3 as the sacrificial agents under visible light irradiation (λ > 420 nm). As illustrated in Fig. 3a, the pristine CdS displayed a poor photocatalytic performance (0.26 μmol g^{-1} h^{-1}), possibly due to the fast charge carrier recombination. After coupling with Ni_3Mo_3N, the CdS showed significantly increased photocatalytic HER activity. Specifically, Ni_3Mo_3N (10 wt%)/CdS with an optimal content of the Ni_3Mo_3N co-catalyst exhibited the highest photocatalytic hydrogen evolution rate of 6.56 mmol g^{-1} h^{-1}, which is much higher than those of CdS and 1 wt% Pt modified CdS. However, further increasing the amounts of

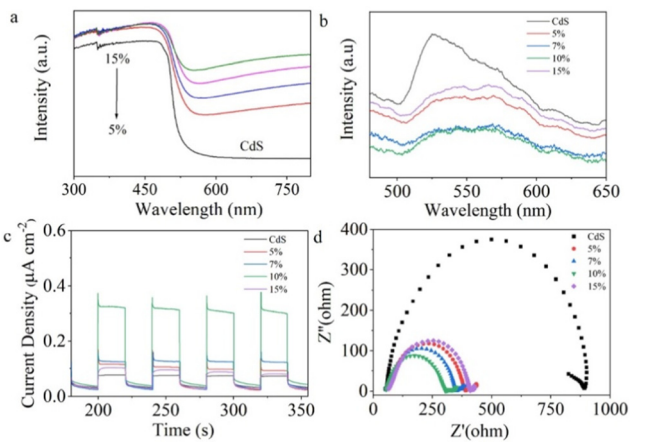

Fig. 2 (a) UV-vis absorption spectra of pristine CdS and Ni_3Mo_3N (x wt%)/CdS (x = 5, 7, 10 and 15) samples; (b) photoluminescence emission spectra of CdS and Ni_3Mo_3N (10 wt%)/CdS samples; photoelectrochemical measurements of CdS and Ni_3Mo_3N (10 wt%)/CdS samples; (c) photocurrent response and (d) EIS Nyquist plots.

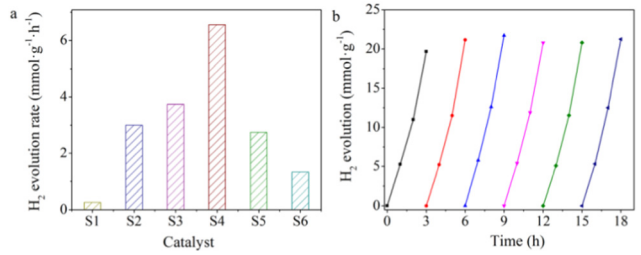

Fig. 3 Photocatalytic performance: (a) photocatalytic H_2 evolution rates of CdS and Ni_3Mo_3N (x wt%)/CdS (x = 0, 5, 7, 10 and 15; S1–S5) samples; Pt (1 wt%)/CdS (S6); (b) cyclic hydrogen evolution over the Ni_3Mo_3N (10 wt%)/CdS sample.

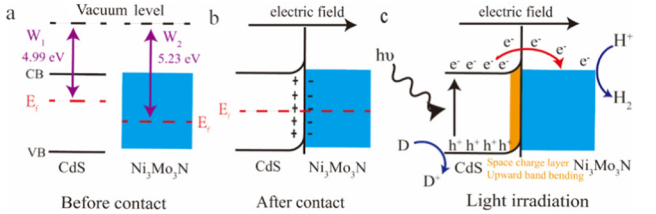

Fig. 4 Schematic illustration of the photocatalytic H_2 evolution and charge transfer process of the Ni_3Mo_3N/CdS composite.

Ni_3Mo_3N in the Ni_3Mo_3N/CdS composite leads to a reduced photocatalytic activity, which could be attributed to the blocking incident light absorption and the coverage of active sites by the excessively loaded Ni_3Mo_3N co-catalyst. In addition, the quantum efficiency of Ni_3Mo_3N (10 wt%)/CdS at 420, 450 and 500 nm was evaluated to 10.6, 8.5 and 6%, respectively (Fig. S3a). Hydrogen cannot be detected under 550 nm light illumination, which confirms that the reactions were driven by photoabsorption of the photocatalyst. The Ni_3Mo_3N (10 wt%)/CdS sample demonstrates a stable photocatalytic hydrogen evolution activity, with no obvious activity loss after six cycling runs (Fig. 3b). Furthermore, we characterized the Ni_3Mo_3N (10 wt%)/CdS sample after six cycling durability tests. The corresponding XRD pattern matches well with the fresh Ni_3Mo_3N (10 wt%)/CdS catalyst, suggesting that its crystallinity and structure are well retained (Fig. S3b). Also, the XPS studies of Ni_3Mo_3N (10 wt%)/CdS before and after the photocatalytic hydrogen evolution stability tests were conducted and the results are shown in Fig. S4 of the SI. It shows that the catalyst is stable under the experimental conditions. Based on the result above, the photocatalytic activity of CdS is actually improved by loading an appropriate amount of Ni_3Mo_3N, and photostability was retained after six cycling runs.

The improvement of the photogenerated charge separation efficiency of CdS by a Ni_3Mo_3N co-catalyst can be ascribed to the Schottky heterojunction between Ni_3Mo_3N and CdS in the composites. To further confirm the direction of photoinduced electron transfer, the surface electronic potentials of CdS and Ni_3Mo_3N were measured using Kelvin probe technology. The work function (WF) of CdS and Ni_3Mo_3N is 4.99 and 5.23 eV, respectively, calculated using the equation: WF (eV) = WF (Au) + CPD/1000. The work function of Ni_3Mo_3N is greater than that of CdS, indicating that the Fermi level of Ni_3Mo_3N is more negative than that of CdS. It is well known that the interfacial electric field is the primary driving force for charge separation (Fig. 4a). When CdS and Ni_3Mo_3N are in contact, the free electrons will transfer from CdS to Ni_3Mo_3N until an equilibrium state is formed, which will induce an interfacial electric field orienting from CdS to Ni_3Mo_3N (Fig. 4b). In addition, the space charge layer formed on the CdS side will cause the band to bend upwards and form the Schottky barrier. The Schottky barrier and band bending effect make charge transfer more effective between Ni_3Mo_3N and CdS, and prevent the electrons captured by Ni_3Mo_3N from returning to CdS. In other words, the Ni_3Mo_3N sides can accumulate negative charges, whereas positive charges accumulate on the CdS side (Fig. 4b). When the Ni_3Mo_3N/CdS composite was under light irradiation, electrons were excited to the conduction band of CdS, leaving the holes in the valence band. The photogenerated electrons migrate to Ni_3Mo_3N driven by the interfacial electric field between CdS and Ni_3Mo_3N. Moreover, the electrons will be captured by the H^+ ions absorbed onto the Ni_3Mo_3N nanoparticles, and hydrogen molecules would form and release on the Ni_3Mo_3N nanoparticle surface (Fig. 4c). The hydrogen molecule is released through one of the two processes: $2H^* \rightarrow H_2 + 2^*$ or $H^+ + e^- + H^* \rightarrow H_2 + *$, where * denotes a catalytically active site on the surface of the Ni_3Mo_3N nanoparticles. Meanwhile, the holes will be consumed by the sacrificial agent. For these reasons, the photogenerated carriers in the CdS were suppressed and the photocatalytic hydrogen evolution was enhanced remarkably.

In conclusion, a noble-metal-free Ni_3Mo_3N/CdS photocatalyst was successfully fabricated, and it showed remarkably enhanced visible light photocatalytic activity for hydrogen evolution. Due to the formation of the Schottky heterojunction between CdS and Ni_3Mo_3N, the migration and separation of photogenerated electron–hole pairs are significantly promoted in the Ni_3Mo_3N/CdS composite. As a consequence, the Ni_3Mo_3N (10 wt%)/CdS composite shows the highest hydrogen evolution rate of 6.56 mmol g^{-1} h^{-1}, which is 25 times higher than that of pure CdS. A high apparent quantum efficiency of 10.6% is reached at 420 nm. Moreover, the photocatalyst also exhibited high photocatalytic activity stability for six consecutive cycles of measurements. This work provides a facile strategy for the synthesis and application of Ni_3Mo_3N nanoparticles as an alternative co-catalyst to Pt in photocatalytic water splitting for hydrogen production.

Conflicts of interest

The authors declare no competing financial interest.

Data availability

The authors confirm that the data supporting the findings of this study are available within the article and its supplemen-

tary information (SI). Supplementary information is available. See DOI: https://doi.org/10.1039/d5dt02653a.

Acknowledgements

This work is funded by the National Natural Science Foundation of China (22108129), Natural Science Foundation of Fujian Province (2025J011078 and 2023J011067), and Scientific Research Fund project of Ningde Normal University (2023ZX02 and 2022FZ23). The Collaborative Innovation Platform Project of Fuzhou-Xiamen-Quanzhou National Independent Innovation Demonstration Zone is acknowledged.

References

1 S. Cao, Y. Chen, C.-C. Hou, X.-J. Lv and W.-F. Fu, *J. Mater. Chem. A*, 2015, **3**, 6096–6101.
2 S. Cao, Y. Chen, C.-J. Wang, P. He and W.-F. Fu, *Chem. Commun.*, 2014, **50**, 10427–10430.
3 A. Pirkarami, S. Rasouli and E. Ghasemi, *Appl. Catal., B*, 2019, **241**, 28–40.
4 L. Chen, H. Huang, Y. Zheng, W. Sun, Y. Zhao, P. S. Francis and X. Wang, *Dalton Trans.*, 2018, **47**, 12188–12196.
5 L. Chen, Y. Zhao, J. Yang, D. Liu, X. Wei, X. Wang and Y. Zheng, *Inorg. Chem.*, 2020, **59**, 1566–1575.
6 C. Bie, B. Zhu, F. Xu, L. Zhang and J. Yu, *Adv. Mater.*, 2019, **31**, 1902868–1902874.
7 L. Shang, B. Tong, H. Yu, G. I. N. Waterhouse, C. Zhou, Y. Zhao, M. Tahir, L.-Z. Wu, C.-H. Tung and T. Zhang, *Adv. Energy Mater.*, 2016, **6**, 1501241–1501248.
8 R. Shi, H. F. Ye, F. Liang, Z. Wang, K. Li, Y. Weng, Z. Lin, W. F. Fu, C. M. Che and Y. Chen, *Adv. Mater.*, 2018, **30**, 1705941–1705947.
9 Q. Sun, N. Wang, J. Yu and J. C. Yu, *Adv. Mater.*, 2018, **30**, 1804368–1804375.
10 S. Guan, X. Fu, Y. Zhang and Z. Peng, *Chem. Sci.*, 2018, **9**, 1574–1585.
11 S. Li, L. Wang, S. Liu, B. Xu, N. Xiao, Y. Gao, W. Song, L. Ge and J. Liu, *ACS Sustainable Chem. Eng.*, 2018, **6**, 9940–9950.
12 B. Ma, H. Xu, K. Lin, J. Li, H. Zhan, W. Liu and C. Li, *ChemSusChem*, 2016, **9**, 820–824.
13 L. Tian, S. Min, Y. Lei, S. Chen and F. Wang, *Chem. Commun.*, 2019, **55**, 6870–6873.
14 K. Zhang, M. Fujitsuka, Y. Du and T. Majima, *ACS Appl. Mater. Interfaces*, 2018, **10**, 20458–20466.
15 C. Wang, W. Qi, Y. Zhou, W. Kuang, T. Azhagan, T. Thomas, C. Jiang, S. Liu and M. Yang, *Chem. Eng. J.*, 2020, **381**, 122611–122620.
16 Z. Sun, H. Chen, L. Zhang, D. Lu and P. Du, *J. Mater. Chem. A*, 2016, **4**, 13289–13295.
17 B. Chang, J. Yang, Y. Shao, L. Zhang, W. Fan, B. Huang, Y. Wu and X. Hao, *ChemSusChem*, 2018, **11**, 3198–3207.
18 L. Yu, Q. Zhu, S. Song, B. McElhenny, D. Wang, C. Wu, Z. Qin, J. Bao, Y. Yu, S. Chen and Z. Ren, *Nat. Commun.*, 2019, **10**, 5106–5116.
19 H. Zhang, P. Zhang, M. Qiu, J. Dong, Y. Zhang and X. W. D. Lou, *Adv. Mater.*, 2019, **31**, 1804883–1804890.
20 D. Gao, J. Zhang, T. Wang, W. Xiao, K. Tao, D. Xue and J. Ding, *J. Mater. Chem. A*, 2016, **4**, 17363–17369.
21 M. Gao, L. Chen, Z. Zhang, X. Sun and S. Zhang, *J. Mater. Chem. A*, 2018, **6**, 833–836.
22 C. Ye, Y. Jiao, H. Jin, A. D. Slattery, K. Davey, H. Wang and S. Z. Qiao, *Angew. Chem., Int. Ed.*, 2018, **57**, 16703–16707.
23 Y. Hou, A. B. Laursen, J. Zhang, G. Zhang, Y. Zhu, X. Wang, S. Dahl and I. Chorkendorff, *Angew. Chem., Int. Ed.*, 2013, **52**, 3621–3625.
24 M. Shao, Y. Shao, S. Ding, R. Tong, X. Zhong, L. Yao, W. F. Ip, B. Xu, X.-Q. Shi, Y.-Y. Sun, X. Wang and H. Pan, *ACS Sustainable Chem. Eng.*, 2019, **7**, 4220–4229.
25 M.-Q. Wang, C. Tang, C. Ye, J. Duan, C. Li, Y. Chen, S.-J. Bao and M. Xu, *J. Mater. Chem. A*, 2018, **6**, 14734–14741.
26 B. Ma, J. Zhang, K. Lin, D. Li, Y. Liu and X. Yang, *ACS Sustainable Chem. Eng.*, 2019, **7**, 13569–13575.
27 A. Wu, Y. Xie, H. Ma, C. Tian, Y. Gu, H. Yan, X. Zhang, G. Yang and H. Fu, *Nano Energy*, 2018, **44**, 353–363.
28 Y. Chen, J. Yu, J. Jia, F. Liu, Y. Zhang, G. Xiong, R. Zhang, R. Yang, D. Sun, H. Liu and W. Zhou, *Appl. Catal., B*, 2020, **272**, 118956.
29 L. An, X. Han, Y. Li, C. Hou, H. Wang and Q. Zhang, *J. Sol-Gel Sci. Technol.*, 2019, **91**, 82–91.
30 R. Kalia, B. M. Pirzada, R. K. Kunchala and B. S. Naidu, *Int. J. Hydrogen Energy*, 2023, **48**, 16246–16258.
31 R. Kalia, P. Yadav, A. Verma, J. Yadav and B. S. Naidu, *J. Alloys Compd.*, 2025, **1015**, 178790.